A Microgravity Flame Speed Study on Refrigerant Mixtures of 2,3,3,3-Tetrafluoropropene (R-1234yf) and Difluoromethane (R-32)

R. Hesse*[1], R. Glaznev[1], C. Schwenzer[1], V. I. Babushok[2], G. T. Linteris[2], H. Pitsch[1], and J. Beeckmann[1]

[1]Institute for Combustion Technology, RWTH Aachen University, Templergraben 64, 52056 Aachen, Germany
[2]National Institute of Standards and Technology, Gaithersburg, MD, USA

Abstract

Today's hydrofluorocarbon (HFC) refrigerants are designed to have a low global warming potential (GWP), resulting in fast atmospheric decomposition and increased reactivity. This causes them to be mildly flammable. The laminar flame speed $S_{L,u}$ ranks refrigerants by their hazardous fire potential. Slowly propagating refrigerants are less hazardous. However, they become affected by gravity and radiation, which raises concerns about their measured flame speeds' reliability. In the present study, we conducted experiments to obtain $S_{L,u}$ of two representative refrigerants, 2,3,3,3-tetrafluoro-1-propene ($CH_2=CFCF_3$, R-1234yf), difluoromethane (CH_2F_2, R-32), and their blends in a drop tower facility providing microgravity to suppress buoyancy. The study reveals that the fire potential of R-1234yf was underestimated by previous experiments.

Introduction

Refrigerants with a high global warming potential (GWP) are replaced with low-GWP substitutes. The reduced atmospheric lifetimes, however, come with mild flammability. Therefore, it is essential to understand their combustion behavior. For safety evaluation, the laminar flame speed $S_{L,u}$ is an important property considering the combustion process's diffusivity, exothermicity, and reactivity. Using $S_{L,u}$ constrains uncertainties of chemical kinetic models.

Reducing the fire-safety hazards of low GWP refrigerants requires flame speeds well below 5 cm/s. Accurate assessment of the combustion characteristics of these refrigerants places particular demands on laminar flame speed measurement methods.

Due to the larger time scales of slowly propagating refrigerant flames, the impact of two physical phenomena dominates: (1) The buoyancy-induced deformation of the flames, and (2) The radiation heat losses, which alter the flame not only on a kinematic but also on a chemical level, disproving conventional flame speed estimates. Hence, accurate literature data on flame speeds for these refrigerants are rare. Generally, it is observed that the lower the fuel's burning rate, the less accurately the combustion behavior can be predicted using chemical kinetic models [1]. Difluoromethane (CH_2F_2, R-32) and 2,3,3,3-tetrafluoro-1-propene ($CH_2=CFCF_3$, R-1234yf, short: "yf") are two low GWP hydrofluorocarbons (HFC) that are of particular interest for the refrigeration industry. R-1234yf is abbreviated with "yf" to improve clarity in graphs and tables.

A refrigerant's burning rate is typically studied in vertical cylindrical tubes (VT) made of glass [2–4] or closed combustion vessels (CV). The latter typically derives the laminar flame speed from the radius evolution of an outwardly propagating flame (OPF) using optical methods (O) like Schlieren or the pressure-rise trace (P) during near isentropic compression. Available flame speed studies on R-32 and R-1234yf are summarized in Tab. 1. The advantages of the CV method are a well-defined measurement environment capable of providing highly accurate data and safe internal treatment of harmful combustion residues. Because of that, it is broadly applied for refrigerant flame speed measurements and will also be used in the present study. Due to limited data availability, chemical kinetic model development for HFC combustion prediction, e.g., by Papas et al. [4] and Babushok et al. [1], partly relies on flame speed data, where radiation, buoyancy, and often stretch effects remain unconsidered (see Tab. 1). This impedes the efforts to develop highly accurate kinetic models. Fewer flame speed data are available for binary or ternary refrigerant mixtures, optimized jointly for cycle efficiency, volumetric capacity, material compatibility, low GWP, low toxicity, and flammability [1].

In our recently published study [11], we focused on assessing robust flame speed measurement methods for slowly propagating refrigerant flames, considering the effects of radiation, stretch, and buoyancy on optical and pressure-rise data. The methods were applied under terrestrial (g) and microgravity (μg) conditions for nitrogen-diluted R-32/air mixtures to mimic the propagation behavior of even slower refrigerants, such as R-1234yf that was reported with a peak $S_{L,u}$ of 1.2 cm/s (cf. Tab. 1). The procedures developed in this study are based on thoroughly identifying data extraction limits and uncertainty estimates for buoyancy, radiation, and stretch effects.

The present paper aims to extend robust flame speed measurements to $CH_2=CFCF_3$/air mixtures and blends with CH_2F_2 and, therefore, continues the investigation under μg. The results will be used to answer the follow-

*Corresponding author: r.hesse@itv.rwth-aachen.de

Table 1: R-32 and R-1234yf refrigerant studies regarding their flame propagation behavior in the Vertical Tube (VT) and Closed Vessel (CV) using either the optical (O) or pressure (P) method to determine $S^0_{L,u}$. g and μg refer to the studies performed under terrestrial gravity and microgravity, respectively.

HFC refrigerant	GWP 100-yr	MW g/mol	T^*_{ad} K	$S^{0,*}_{L,u}$ cm/s	Configuration		Rad. cor.	p bar	T K	ϕ -	$X_{O2,air}$ -	Ref.
R-32	677	52.024	2207	6.7[a]	VT	g	N/A	1.01	298	0.89-1.6	0.21	[2–4]
CH_2F_2					CV-P/O	g	N/A	1.01	298	0.76-1.5	0.21	[5, 6]
					CV-P/O	$g/\mu g$	N/A	1.01	298	0.83-1.27	0.21	[6]
					CV-P	g	OTM	1.01/3	298/400	0.9-1.4	0.21	[7, 8]
					CV-O	g	OTM	1.01-3	298/333	0.9-1.6	0.21	[9, 10]
					CV-P/O	$g/\mu g$	OTM	3	333	1.3	0.16-0.21	[11]
R-1234yf	4	114.04	2047	1.2[b]	VT	g	N/A	1.01	298	1.0	0.21	[4]
CH_2=$CFCF_3$					CV-P	g	N/A	1.01	298	0.8-1.55	0.21-0.5	[12, 13]
short "yf"					CV-P/O	$g/\mu g$	N/A	1.01	298-353	1.05-1.78	0.21	[14]

* At peak laminar flame speed in mixtures with dehumidified air under 1 atm, 298 K
[a] From ref. [5]; [b] From ref. [12];

ing research questions: How do stretch and radiation behavior differ of R-32 and R-1234yf-blends? How much is the fire hazardous potential decreased if R-1234yf instead of R-32 is used? How well do chemical kinetic models predict the blending behavior?

Experimental Apparatus and Procedures

Microgravity experiments were conducted in ZARM's (Center of Applied Space Technology and Microgravity) prototype high-repetition drop tower facility called the GraviTower Bremen Pro (GTB Pro) providing up to 2.5 s weightlessness of less than 10^{-4} g during drops. The flame speed setup, integrated into a capsule with a payload height of 953 mm, is accelerated with a rope drive, describing a parabolic motion. The capsule is fixed on an air cushion from which it detaches during the flight. The outer slider protects the capsule from air drag during flights.

The flame speed setup, illustrated in Fig. 1, consists of a spherical combustion chamber with an inner diameter of 100.5 mm. The Schlieren arrangement was installed vertically in a dual-field configuration with a CMOS camera at the top and a high-power LED emitting green light at the bottom. The

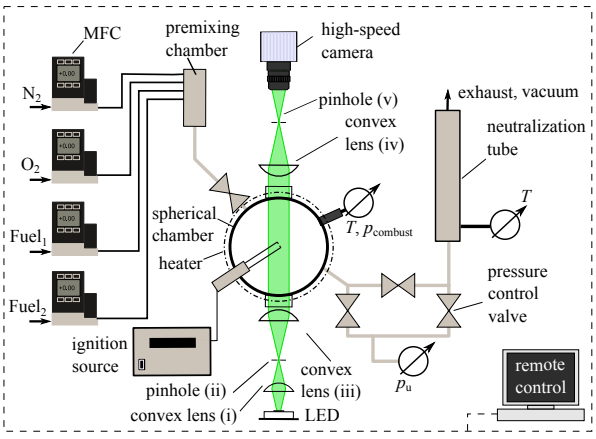

Figure 1: Experimental setup for flame speed measurements using the optical and the pressure method under 1-g and μg conditions.

interior of the chamber is illuminated by parallel light via two 50 mm cylindrical windows made from sapphire crystal located on opposite sides. Flame images with a size of 800×832 pixels were recorded at 10000 frames per second (fps), providing a spatial resolution of 17.36 pixel/mm.

The mixture preparation significantly influences the accuracy of flame speed experiments. Here, the maximum uncertainty in equivalence ratio is 0.02 and 0.2 % in X_{O_2}. The oxidizer was prepared from nitrogen and oxygen, each with a purity of 99.999 %. R-32 and R-1234yf had a purity of 99.5 %. The gases are carried along in separate gas cylinders mounted to a mixture preparation platform.

A vacuum pump is used to evacuate residual gases from the vessel and tube network, followed by the filling process via an additional premixing chamber. The process is controlled remotely with solenoid valves, MFCs, and a pressure-regulating valve at the chamber outlet. They are closed simultaneously once the set-point ignition pressure has been maintained for sufficient mixing time. An appropriate settling time of 5 min is followed by ignition. A two-step coil and capacitor ignition system provides spark energies up to 5 J. Sparks are discharged through elongated spark plug electrodes with diameters of 0.3 mm and gaps between electrode tips of 2 mm. Minimum ignition energies were approached by gradually increasing ignition energies in the laboratory framework to limit the effect on flame evolution. Earlier studies used thicker electrodes with a diameter of 1 mm, resulting in more substantial conductive heat losses. By using much thinner electrodes, ignition energies and, thus, the influence on the flame propagation could be reduced.

Toxic combustion products like hydrogen fluoride (HF) are treated internally in a soda-lime bath. A high-accuracy Keller 35XHTC and a high-frequency Kistler 4011A pressure transducer were used for measuring the ignition and combustion pressure, respectively. Pressure data were recorded at 10000 Hz. The combustion chamber and its periphery can be heated for measurements at elevated temperatures. The present study obtained results with varying R-32/R-1234yf blending ratios and

equivalence ratios of $\phi = 1.087$ and 1.284 at $p_0 = 3\,\mathrm{bar}$ and $T_0 = 333\,\mathrm{K}$ and corresponding p and T along the near-isentropic pressure-rise. The global conversion reaction for $CH_2F_2/CH_2{=}CFCF_3$ blends is given by

$$\begin{aligned} X_{\mathrm{yf}}\cdot CH_2{=}\,CFCF_3 + (1-X_{\mathrm{yf}})\,CH_2F_2 \\ + (1+1.5X_{\mathrm{yf}})\,O_2 \\ = 2\,HF + X_{\mathrm{yf}}\cdot\,CF_2O + (1+X_{\mathrm{yf}})\,CO_2. \end{aligned} \quad (1)$$

X_{yf} is the molar fraction of R-1234yf in the refrigerant blend with R-32. Carbonyl fluoride (CF_2O) is a toxic combustion product that is absent in the oxidation of R-32 but is available in large fractions in the blend's products.

Flame Speed Determination

Optical method

Flame front extraction is limited to spherically smooth flame fronts above a critical radius associated with the complete decay of ignition artifacts and within a quasi-isobaric regime. Backgrounds are removed from Schlieren images, and the flame front is obtained using the method of Otsu et al. [15]. This provides the temporal evolution of the flame radius R_f at its iso-temperature surface of 840 K [16]. Central differences are applied to obtain the stretched propagation speed of a burned mixture $S_{\mathrm{L,b}} = \dot{R}_\mathrm{f} = \mathrm{d}R_\mathrm{f}/\mathrm{d}t$. An OPF's stretch rate K is defined as the temporal change of the flame surface area A leading to $K = 1/A \cdot \mathrm{d}A/\mathrm{d}t = 2/R_\mathrm{f} \cdot \mathrm{d}R_\mathrm{f}/\mathrm{d}t$. The nonlinear expression provided by Kelley et al. [17] is used to calculate the unstretched flame speed $S^0_{\mathrm{L,b}}$ denoted with the superscript "0" and the Markstein length $\mathscr{L}_\mathrm{b}$. The unstretched laminar flame speed of the unburned gas, $S^0_{\mathrm{L,u}}$, can be evaluated for adiabatic flames by mass continuity through a planar unstretched flame, $S^0_{\mathrm{L,u}} = S^0_{\mathrm{L,b}}(\rho_\mathrm{b}/\rho_\mathrm{u})$, where ρ_b and ρ_u are the burned and unburned densities. A slowly burning flame can render this relation invalid due to radiation heat loss, as discussed in [9]. In the present study, only data obtained with the pressure method are corrected for radiation heat loss.

Pressure method

Several assumptions are invoked to calculate $S_{\mathrm{L,u}}$ from pressure-rise data, including infinitely thin smooth spherical flame fronts during combustion, spatially uniform pressure during combustion, isentropic compression of unburned gases, ideal combustion of both burned and unburned gases, and negligible radiation and buoyancy effects. In Bariki et al. [18], we recently discussed this method and its errors in fast-burning flames using a two-zone model. For slowly burning flames, as investigated in the present study, a multi-zone model, such as the Mass- and Energy-Conserving Thermo (MECT) introduced by Elia et al. [19], is required to incorporate radiation heat losses. These alter the flame temperature more, as can be represented by two zones. Here, we selected the National Institutes of Standards and Technology's (NIST) data reduction tool for spherical constant volume flame experiments [20], which uses the MECT multi-zone model. The pressure data were processed by applying a moving average scheme. Radiation effects were modeled for species in the burned equilibrated gas, CO_2, CO, H_2O, CF_2O, and HF, using the optically thin model (OTM), thus assuming the absence of radiation absorption. Handling radiation in a statistical narrow-band model framework is impossible due to the lack of radiation absorption parameters at appropriate combustion temperatures.

Numerical Framework

Flame speed simulations of planar stationary flames were performed using the open-source code FlameMaster [21]. Domain sizes were enlarged to 0.5 m resolved by 5000 grid points to visualize oxidation effects far from the reaction zone. The mesh is refined in the reaction zone. Simulations were performed using the recently developed chemical kinetic model by Babushok et al. [22] containing 113 species and 2059 elementary reactions, forward and backward reactions counted separately.

Results and Discussions

The results section is structured as follows: First, the optical data is analyzed for its flame morphology and propagation speed. Second, the pressure-rise data is added to discuss the blending effects of R-32/R-1234yf/air mixtures compared to simulations. Third, flame speed correlations are presented for kinetic model refinement.

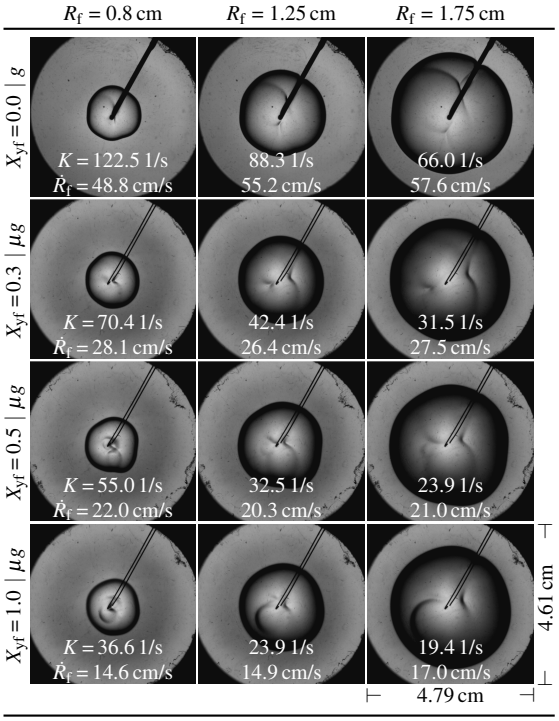

Figure 2: Raw flame recordings at $\phi = 1.087$, $X_{\mathrm{O_2,ox}} = 21.14\,\%$, 333 K and 3 bar at the volume equivalent flame radius R_f.

Flame Morphology and Propagation Speed

Figure 2 depicts the flame evolution of R-32/R-1234yf/air mixtures with varying blending ratios X_{yf} at an equivalence ratio of 1.087 obtained with the optical method. R-32/air flames propagate significantly faster than R-1234yf/air flames and, therefore, were recorded under normal gravity (g). The flames expand spherically without apparent artifacts caused by the electrodes. Furthermore, despite the fact that the present study was conducted at high ignition pressures of $p0 = /unit[3][bar]$, flame wrinkling due to hydrodynamic or thermodiffusive instability is not an issue. This also applies to richer flames of $\phi = 1.284$ and elevated pressures along the near-isentropic compression, relevant for pressure-rise data evaluation. The flame propagation speed of neat R-32/air mixtures is about three times faster than that of neat R-1234yf/air mixtures (cf. $R_f = 1.75\,cm$). The relationships between the propagation speed $\dot{R}_f$ and stretch rate K are shown in Fig. 3 for $\phi = 1.087$ (top) and 1.284 (bottom). Symbols represent experiments, dashed lines the mean nonlinear extrapolation to zero stretch rate, colored hues the 1σ confidence interval considering extrapolation of an entire data set, and dashed lines flame iso-radii at 0.5, 1.0, and 2 cm. The correction of radiation heat loss was omitted to analyze the data in its original state. The flame propagation can be subdivided into three regimes associated with ignition energy decay (I), transition to self-sustained propagation (II), and self-sustained flame propagation (III). In the case of R-1234yf/air mixtures, flames propagate intrinsically at $R_f > 1\,cm$, marking the lower extrapolation limit to zero stretch rate. The extrapolation's slope at the y-axis intercept represents the Markstein length $\mathscr{L}_b$, which increases toward leaner mixtures. Additionally, Markstein lengths first decrease with increasing X_{yf} and then drastically increase approaching $X_{yf} = 1.0$. At $\phi = 1.284$, blends with X_{yf} ranging from 0.3 to 1.0 approach almost identical unstretched propagation speeds. However, their Markstein lengths differ significantly.

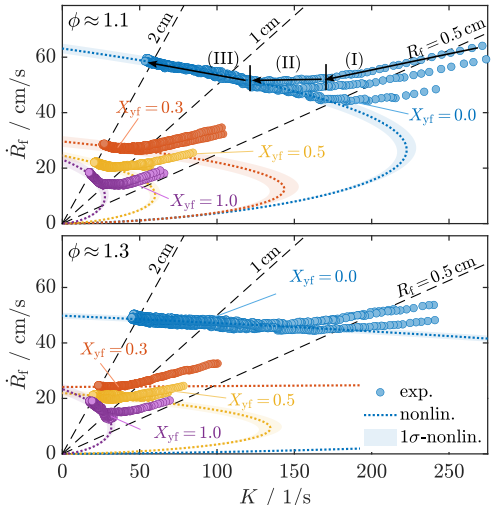

Figure 3: Propagation speed-stretch rate dependence at 3 bar, 333 K, $\phi = 1.087$ (top), and $\phi = 1.284$ (bottom) with increasing R-1234yf mole fraction X_{yf}.

In Fig. 4, R-1234yf-flames of the present study at 3 bar and 333 K and by Takizawa et al. [12] at 1 atm and 298 K, both acquired under μg, are compared. Set equivalence ratios between both works deviate slightly (cf. $\phi = 1.0$ and 1.33 [12]), which disappears in the already low equivalence ratio sensitivity of R-1234yf/air mixtures. Contrary to our findings, Takizawa et al. observed a Markstein length decrease toward lean mixtures. A closer look reveals a propagation speed increase for the $\phi = 1.0$ mixture at a flame radius of 2 cm. The authors excluded this data range since it was found to be an 'irregular increase' unsuitable for extrapolation to zero stretch rate. Our recent findings show that $\mathscr{L}_b$ is strictly positive at an elevated pressure of 3 bar and should even increase at atmospheric pressure due to the increased flame thickness. This indicates that the 'increase' can be interpreted as the transitioning regime (II) into self-sustained flame propagation (III), and no valid extrapolation range can be identified. Therefore, the hazardous fire potential of R-1234yf might be underestimated by previous works.

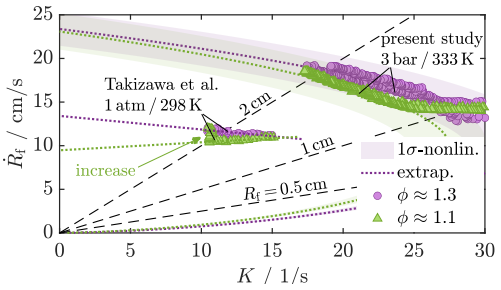

Figure 4: Neat R-1234yf's propagation speed-stretch rate dependence at 3 bar, 333 K, $\phi = 1.087$, and 1.284 (present study) in comparison to measurements by Takizawa et al. [12] at 1 atm, 298 K and slightly different $\phi = 1.0$, and 1.33.

Blending Effect

In addition to the propagation speed analysis using the optical method, flame speeds are extracted along the near-isentropic compression using the pressure method. This data are already converted to the unburned conditions, so we refer to it as the laminar flame speed $S_{L,u}$. Note that $S_{L,u}$ is not strictly referring to the unstretched laminar flame speed $S^0_{L,u}$, as it might still be stretch-affected at small flame radii and corresponding low pressures. To prevent this, stretch-unaffected data must be selected and extrapolated to the initial conditions at p_0 and T_0. A lower limit of $p > 1.8p_0$ was found to satisfy this demand, which can be verified with $S^0_{L,u}$ from the optical method. The upper limit is associated with the inflection point of the pressure-time history to exclude flame wall interactions.

Results for $\phi = 1.087$ with increasing X_{yf} are shown in Fig. 5. All graphs share the same pressure axis ranging from 2 to 14 bar but reach slightly deviating unburned temperatures at these pressures, displayed by the top-side x-axis. The pressure-rise data, denoted with

'$|_p$', are post-processed under the adiabatic (ADI) and optically thin model (OTM) radiation assumptions, represented by blue and red colors, respectively. Thus, OTM refers to the radiation-corrected flame speed. Symbols and solid lines, respectively, represent experimental data and fitted splines. Black circles, labeled with '$|_o$', are unstretched $S^0_{L,u}$ results using the optical method and the adiabatic assumption. A power-law correlation for the dependence of temperature and pressure is commonly used to fit laminar flame speeds, written as

$$S_{L,u} = S_{L,u,0}\left(\frac{p}{p_0}\right)^{\alpha}, \text{ where } \quad T = T_0\left(\frac{p}{p_0}\right)^{\frac{\gamma-1}{\gamma}}, \quad (2)$$

where $S_{L,u,0}$ is the laminar flame speed at initial conditions p_0 and T_0, and the exponent α depends on the mixture composition. The temperature T in the second equation corresponds to the laminar flame speed $S_{L,u}$ and pressure p. In Fig. 5, power law results are shown as dashed lines with error bars that combine experimental and extrapolation uncertainties and yield the power law correlation's 95 % confidence interval (CI). Power law results for the OTM assumption are given in Table 2. Laminar flame speeds at the initial conditions are labeled in the graphs, showing matching flame speeds of the optical and pressure method assuming adiabatic gas. The radiation effect increases from about 15 % at X_{yf} to 25 % with increasing R-1234yf-content.

In order to benchmark the predictions of Babushok et al.'s chemical kinetic model [22], the radiation-corrected data is compared to adiabatic planar stationary flame simulations, denoted by dotted lines. Flame speeds were calculated at the power law correlation's pressures and temperatures given by Eq. 2 and Table 2. Whereas $S^0_{L,u}$-predictions at the initial conditions of the neat refrigerants are within the uncertainty limits, blends, especially $X_{yf} = 0.3$, are over-predicted. This changes with increasing pressure and temperature so that, eventually, blends are predicted within their uncertainty, and neat refrigerants are under-predicted. However, elevated pressures have little application relevance for refrigerants but enable us to extract robust flame speed data without Markstein effects.

In Fig. 6, $S^0_{L,u}$ are shown against the blend's mole fraction X_{yf} at p_0 and T_0 of 3 bar, 333 K (left), and 6 bar, 389 to 398 K (right). Again, flame speeds recorded by Takizawa et al. [14] under μg are added for reference. Simulations are depicted by dotted lines. Both data sets show a significant drop in the flame speed when 30 % of R-32's mole fraction is replaced by R-1234yf. Here, the kinetic model under-predicts this drop, leading to higher flame speeds of the $X_{yf} = 30$ % blend. Takizawa's results indicate that R-1234yf burns with one-fourth of R-32's flame speed. The present study shows that R-1234yf burns with half R-32's flame speed. This corresponds to a significantly increased fire hazardous risk of R-1234yf, also predicted by the kinetic model.

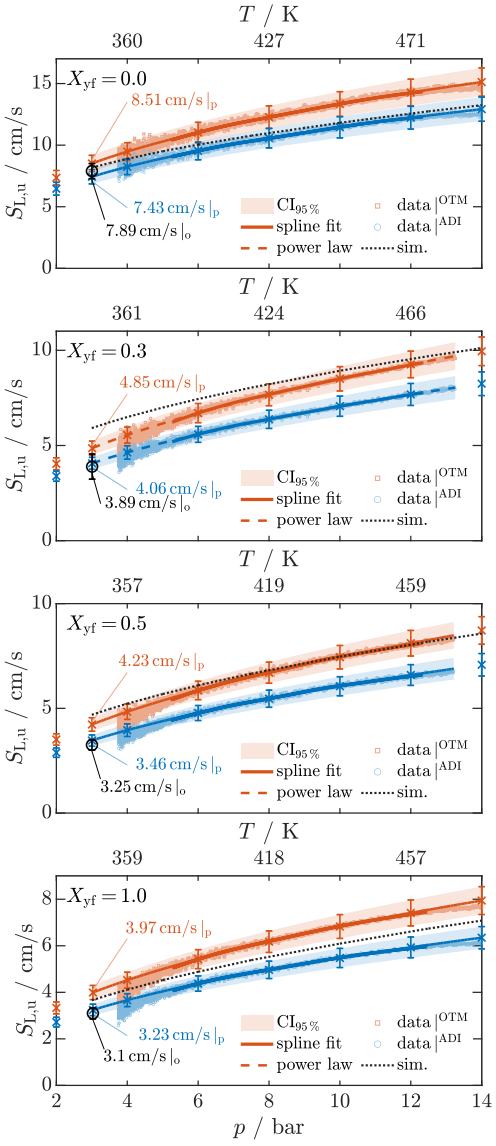

Figure 5: R-32/R-1234yf/air mixtures at 3 bar, 333 K, and $\phi = 1.087$. The subscripts 'o' and 'p' refer to the optical and pressure methods. The superscripts 'ADI' and 'OTM', denote the adiabatic and optically thin model gas assumptions.

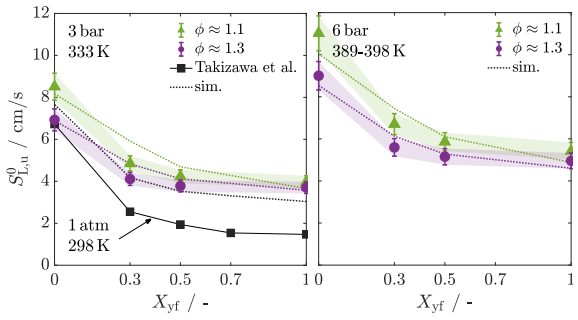

Figure 6: Flame speeds of R-32/R-1234yf/air mixtures for $\phi = 1.087$ and 1.284 at p_0 and T_0 of 3 bar, 333 K (left), and 6 bar, 389 to 398 K (right). Data by Takizawa et al. [14] are shown for reference at 1 atm, 298 K for equivalence ratios at peak $S^0_{L,u}$. The dotted lines are simulations.

Table 2: Power law results for Eq. (2) with OTM assumption.

X_{yf} -	ϕ -	$S_{L,u,0}$ cm/s	T_0 K	p_0 bar	p_{lim} bar	α -	γ -
0.0	1.087	8.51	336.8	3.0	12.3	0.373	1.324
0.3	1.087	4.85	337.0	3.0	12.4	0.466	1.303
0.5	1.087	4.23	334.6	3.0	12.3	0.470	1.296
1.0	1.087	3.97	336.5	3.0	12.4	0.450	1.284
0.0	1.284	6.93	336.4	3.0	12.2	0.377	1.317
0.3	1.284	4.11	336.9	3.0	12.3	0.445	1.294
0.5	1.284	3.78	335.9	3.0	12.4	0.447	1.285
1.0	1.284	3.70	335.6	3.0	12.4	0.422	1.273

Summary and Conclusions

The presented approach eliminates gravity-induced flame buoyancy under μg, corrects radiation heat losses, and minimizes stretch effects by restricting the valid data range for extrapolations. As a result, experiments could be conducted with unmatched accuracy for these challenging substances and conditions. Compared to available literature data, the present study reveals an increased fire-hazardous potential of R-1234yf/air mixtures and their blends with R-32. Still, flame speed calculations with the chemical kinetic model by Babushok et al. [22] could predict the neat refrigerants' and their blends' flame speeds at most conditions measured in the present study. Some deviations above experimental uncertainty limits exist in the sub-linear blending behavior at around $X_{yf} = 0.3$ and at higher pressures. The latter, relevant for down-scaling from higher to atmospheric pressures, could be improved by updating the base chemistry. Next, sensitivity and pathway analysis must be performed to identify potential model improvements for the blending effect. The flame structure and Lewis number effects will also be analyzed to improve the understanding of ignition and oxidation mechanisms. Furthermore, according to the kinetic model, the combustion products contain similar concentrations of CF_4 as CF_2O. Therefore, its contribution to radiation heat losses must be checked.

Acknowledgement

The authors from RWTH gratefully acknowledge the financial support partly provided by the Deutsches Zentrum für Luft und Raumfahrt (DLR, German Aerospace Center), Grant no. 50WM2073 and the National Institute of Standards and Technology (NIST), Grant no. 70NANB21H157. Co-authors from NIST obtained financial support under contract DE-EE0007615 from the Office of Energy Efficiency and Renewable Energy, U.S. Department of Energy. We thank the European Space Agency (ESA) for funding and the Center of Applied Space Technology and Microgravity (ZARM) for providing the drops in the GTB Pro.

References

[1] V. Babushok, D. Burgess, D. Kim, M. Hegetschweiler, and G. Linteris, *Tech. Rep.* (2021).

[2] D. Clodic and T. Jabbour, *HVAC&R Research* **17**, 51 (2011).

[3] K. Takizawa, N. Igarashi, K. Tokuhashi, S. Kondo, M. Mamiya, and H. Nagai, *ASHRAE Trans.* **119**, 255 (2013).

[4] P. Papas, S. Zhang, W. Kim, S. Zeppieri, M. Colket, and P. Verma, *Proc. Combust. Inst.* **36**, 1145 (2016), ISSN 1540-7489.

[5] K. Takizawa, A. Takahashi, K. Tokuhashi, S. Kondo, and A. Sekiya, *Combust. Flame* **141**, 298 (2005), ISSN 0010-2180.

[6] K. Takizawa, S. Takagi, K. Tokuhashi, S. Kondo, M. Mamiya, and H. Nagai, *ASHRAE Trans.* **119**, 243 (2013).

[7] R. R. Burrell, J. L. Pagliaro, and G. T. Linteris, *Proc. Combust. Inst.* **37**, 4231 (2019), ISSN 1540-7489.

[8] D. R. Burgess, R. R. Burrell, V. I. Babushok, J. A. Manion, M. J. Hegetschweiler, and G. T. Linteris, *Combustion and Flame* **236**, 111795 (2022), ISSN 0010-2180.

[9] R. Hesse, L. Berger, C. Bariki, M. J. Hegetschweiler, G. T. Linteris, H. Pitsch, and J. Beeckmann, *Proc. Combust. Inst.* **38**, 4665 (2021).

[10] M. J. Hegetschweiler, J. L. Pagliaro, L. Berger, R. Hesse, J. Beeckmann, H. Pitsch, and G. T. Linteris, *Sci. Technol. Built Environ.* **3**, 1 (2020).

[11] R. Hesse, C. Bariki, M. J. Hegetschweiler, G. T. Linteris, H. Pitsch, and J. Beeckmann, *Proc. Combust. Inst.* **39** (2022), ISSN 1540-7489.

[12] K. Takizawa, K. Tokuhashi, and S. Kondo, *J. Hazard. Mater.* **172**, 1329 (2009), ISSN 0304-3894.

[13] K. Takizawa, E. Hihara, C. Dang, and M. Ito, *JSRAE Final Report* (2017).

[14] K. Takizawa, in *Int. Symp. Next-gen. Air-Con. Refrig Technol.* (2010).

[15] N. Otsu, *IEEE Trans. Syst. Man Cybernetics* **9**, 62 (1979).

[16] D. Dunn-Rankin and F. Weinberg, *Combust. Flame* (1998).

[17] A. Kelley, J. Bechtold, and C. Law, *J. Fluid Mech.* **691**, 26 (2012), ISSN 1469-7645.

[18] C. Bariki, R. Hesse, F. Halter, H. Pitsch, and J. Beeckmann, *Proc. Combust. Inst.* **38**, 2185 (2021), ISSN 1540-7489.

[19] M. Elia, M. Ulinski, and M. Metghalchi, *J. Eng. Gas Turbines Power* **123**, 190 (2000), ISSN 0742-4795.

[20] M. Hegetschweiler and G. T. Linteris, *NIST Technical Note in preparation* 999 (2021).

[21] H. Pitsch, Flamemaster (1998), `https://www.itv.rwth-aachen.de/downloads/flamemaster/`.

[22] V. Babushok, D. Burgess Jr, M. Hegetschweiler, and G. Linteris, *Combust. Sci. Technol.* 1–24 (2020).